The effect of Majorana fermions on the Andreev spectroscopy applied to topological multiband superconductors

Ana Cristina Silva
Under the supervision of: M.A.N. Araújo and P.D. Sacramento

Instituto Superior Técnico, Lisboa, Portugal

October 2014

Abstract

The differential conductance between a normal metal and a two-band topological superconductor is studied. To address the wavefunction's matching conditions at the interface, the extension of quantum waveguide theory to the Andreev scattering problem is applied. For a normal metal-superconductor junction, the scattering mechanism known as the Andreev reflection will occur for small energy bias. It can be briefly defined as the process in which an incident electron will be reflected back as hole, with the transmission of a Cooper pair into the superconductor's side. A topological superconductor is characterized by the existence of zero-energy conducting states at the interface which can be identified as Majorana fermions. To represent this system we considered a Hamiltonian model in which the Bogoliubov-De Gennes matrix will split into two 4×4 matrices. Considering only one of these two subspaces the subsystem can be tuned either to a trivial or topological phase by altering one of the band structure parameters and keeping the remaining parameters fixed. The topological phase will be characterized by a non-zero Chern number. As this quantity can be related to the number of edge-states by the bulk-boundary correspondence, its value gives the number of localized Majorana fermions. The calculated differential conductance within the framework of quantum waveguide theory is shown to be consistent with the topological index, in contrast with the historically established Blonder-Tinkham-Klapwijck model, and it also reveals the existence of destructive interference effects, which cannot be attained if the conduction paths are treated independently.

Keywords: Quantum waveguide theory, Majorana fermion, topological superconductor, Andreev bound state, differential conductance

1. Introduction

1.1. An introduction to Topological band theory

The building blocks of matter can interact in various forms, which subjected to certain external conditions, can lead to different states of matter. In the theory of phase transitions, one usually defines a local order parameter which acquires a distinct expectation value as the different phases are established. By comparison with this framework, topological states of matter emerge as a new paradigm [1] : not only is it impossible to define a local order parameter, but also the different topological states are differentiated upon the inability to adiabatically deform the energy bands into one another, without closing the bulk gap. Thus, a material in a topological phase, in contact with another in a trivial phase, has to undergo a phase transition at the interface, accomplished by the vanishing of the bulk gap. At the points where the bulk gap collapses, gapless conducting states arise. These states are, therefore, able to conduct current along the interface and are known as edge-states [2, 3]. This scenario can occur, for example, at the interface between a topological insulator and the vacuum. In this case, one can see more easily that the appearance of such edge-states is highly interconnected to the non-trivial topology of the bulk, a phenomena known as bulk-edge correspondence [2].

The gapless modes exhibit more robustness in face of local disorder, which is another peculiarity of the topological phase, and are related with the existence of a non-zero topological invariant [4].

Here, the dominant focus falls to one topological invariant, the Chern number, present in systems without time-reversal symmetry.

The mathematical construction of the Chern number is rooted in the Berry phase [5]. Nevertheless, in a system where the interface demarks the separation between a trivial and a topological phase, the Chern number can also be attained through the bulk-boundary correspondence [2], which math-

ematically is stated in the following way: if there are N_R edge states with positive group velocity and N_L with negative, the change in the Chern number across the interface will be quantified by

$$\Delta C = N_R - N_L \ . \tag{1}$$

Provided that two physical systems share the same topological invariant, they are topologically equivalent, which suggests that there must be some underlying symmetries enabling the division of systems into topological classes [6].
In the case of the superconductor's Hamiltonian, written in the general form:

$$\hat{\mathbf{H}} = \frac{1}{2}\sum_{\mathbf{k}} \hat{\mathbf{a}}^{\dagger}_{\mathbf{k}}.\ \mathcal{H}_{BdG}\ .\hat{\mathbf{a}}_{\mathbf{k}}\ ,\ \mathcal{H}_{BdG} = \begin{bmatrix} \hat{\Xi} & \hat{\Delta} \\ \hat{\Delta}^{\dagger} & -\hat{\Xi}^{*} \end{bmatrix}\ , \tag{2}$$

where $\hat{\mathbf{a}}_{\mathbf{k}} = (\hat{c}_{\mathbf{k}\uparrow} \quad \hat{c}_{\mathbf{k}\downarrow} \quad \hat{c}^{\dagger}_{-\mathbf{k}\uparrow} \quad \hat{c}^{\dagger}_{-\mathbf{k}\downarrow})^{T}$, the Bogolubov-De Gennes Hamiltonian ($\mathcal{H}_{BdG}$) written as in eq(2) has particle-hole symmetry (PHS), defined as [6]:

$$\mathcal{H}_{BdG}(\mathbf{k}) = -\tau_x \mathcal{H}^{*}_{BdG}(-\mathbf{k})\tau_x \tag{3}$$

where the Pauli matrix τ_x operates in particle-hole space. This is an intrisic symmetry of the $\mathcal{H}_{BdG}$ matrix in eq(2) due to the Hermiticity of Ξ and because $\hat{\Delta}(\mathbf{k}) = -\hat{\Delta}^{T}(\mathbf{k})$, by imposition of the Fermi statistics [7, 6]. The Hamiltonian in eq(2) can be diagonalized by performing a Bogolubov transformation, allowing to express the Hamiltonian in terms of the non-interacting quasiparticle operators [8]. In real space the quasiparticle destruction operator will be:

$$\hat{\gamma} = \int d\mathbf{r}\ u^{*}_{\uparrow}(\mathbf{r})\hat{\psi}_{\uparrow} + u^{*}_{\downarrow}(\mathbf{r})\hat{\psi}_{\downarrow} + v^{*}_{\uparrow}(\mathbf{r})\hat{\psi}^{\dagger}_{\uparrow} + v^{*}_{\downarrow}(\mathbf{r})\hat{\psi}^{\dagger}_{\downarrow}\ , \tag{4}$$

where the operators ψ and $\psi^{\dagger}$ are the annihilation/creation operators for fermions in real space and can be attained from the usual momentum operators, c and $c^{\dagger}$, by a Fourier transform operation [8].

The eigenstates of the $\mathcal{H}_{BdG}$ are given by: $\phi(\mathbf{r}) = (u_{\uparrow}(\mathbf{r}) \ \ u_{\downarrow}(\mathbf{r}) \ \ v_{\uparrow}(\mathbf{r}) \ \ v_{\downarrow}(\mathbf{r}))^{T}$. Eq(3) implies that if the eigenstate ϕ has energy E, the eigenstate $\tau_x\phi^{*}$ will have $-E$ energy. Thus, if $E = 0$ and this is a non-degenerate state, PHS will lead to:

$$\phi(\mathbf{r}) = \tau_x\phi^{*}(\mathbf{r}) \Leftrightarrow \hat{\gamma} = \hat{\gamma}^{\dagger} \Rightarrow \text{Majorana fermion}\ . \tag{5}$$

In analogy with particle physics, this equality can be viewed as the equivalence between particle and anti-particle and thus the operator represents a Majorana fermion. Conversely, it is possible to describe an usual fermion as superposition of Majorana modes [9, 10, 3]. This can be clarified by constructing an algebraic representation where the usual fermionic operators are written in terms of Majorana operators (eq(5)), which satisfy [9, 10, 11]:

$$\{\gamma_i, \gamma_j\} = 2\delta_{ij}\ . \tag{6}$$

A question that can then arise is whether it will be possible to have single Majoranas in a superconductor, without them pairing up to form an usual fermion. This indeed is accomplishable in a topological superconductor, where they will appear as edge states bounded to an interface delimiting a topological phase transition [3, 9, 10, 11].

1.2. **Andreev spectroscopy**

When a normal metal and a superconductor are in close vicinity, new features of electronic transport can be observed. The proximity between the two structures is mediated by an interface, which may or may not include a tunnel barrier. In the absence of such barrier, the interface is called a microconstriction - an inter-metalic point contact [12]. Different electronic transport mechanisms are privileged whether the interface is a 'pure' point contact or a tunnel barrier. In the first case, the predominant process of scattering is the Andreev reflection, which can be understood in the following way: an incoming electron from the normal metal, with energy below the superconducting gap Δ , tries to propagate through the interface to the superconductor region. The only way the superconductor can accommodate a freely propagating quasiparticle excitation is in the energy states above the superconducting gap, which means the incoming excitation from the normal metal can only be transmitted if it exponentially decays to the ground state [12, 13]. This is accomplished by a process of condensation of the first electron with another electron of the normal metal to form a Cooper pair [13]. The second electron can be viewed as reflecting a hole back to the normal metal, and so the Andreev reflection can be briefly defined as a process of reflection of an electron into a hole, with the transmission of a Cooper pair into the superconductor's side [12].
In 1982, Blonder, Tinkham and Klapwijk (BTK) constructed a theory in which the differential conductance of a normal-superconductor junction could be determined for various kinds of interfaces, ranging from a point contact microconstriction to a tunneling junction [13]. The variation from both regimes was successfully accomplished by introducing a localized repulsive potential at the interface, with a strength controlled by a dimensionless parameter, Z. This theory was devised for s-wave superconductors. In fact, different behaviours can arise as soon as the pairing symmetry is modified and d-wave superconductivity is a good example of such, with the appearance of zero-energy localized

sates at the interface known as Andreev bound states (ABS) [15, 14].
In 1996, Kashiwaya,Tanaka and Kajimura developed a generalization of the BTK framework for anisotropic superconductors [14]. The authors found that, for d-wave superconductivity, the presence of ABS have an impact on the differential conductivity: an enhanced peak for finite strength barriers will be located at zero bias, a phenomena known as zero-bias anomaly or zero-bias conductance peak (ZBCP).
The above presented theories for studying the differential conductance in a normal metal-superconductor junction have been developed in the assumption of one band superconductors. As the incoming normal metal electron now approaches the superconductor it will encounter two possible electron-pockets enabling transmission, meaning that there are two channels for the transmission into the superconductor [16].
A simple way to address the problem is to apply the anisotropic version of the BTK theory separately to the two bands and then add them together, therefore treating the multiband superconductor as a parallel conductor [17]. This, however neglects any possible quantum mechanical interference effects that may occur at the interface, urging for a new approach. This issue has close resemblance with a quantum waveguide problem [18], which lead the authors M.A.N. Araújo and P.D.Sacramento to adapt the model of a quantum waveguide to the interface between a normal-metal and a multiband superconductor [19, 16].

2. The model for the Hamiltonian

One shall consider a topological superconductor with two orbitals per lattice site described by the particle-hole symmetric Hamiltonian:

$$\hat{H} = \frac{1}{2}\sum_{\mathbf{k}} (\hat{\mathbf{c}}^\dagger \;\; \hat{\mathbf{c}}) \begin{bmatrix} \Xi(\mathbf{k}) & \hat{\Delta}(\mathbf{k}) \\ \hat{\Delta}^\dagger(\mathbf{k}) & -\Xi^*(-\mathbf{k}) \end{bmatrix} \begin{pmatrix} \hat{\mathbf{c}} \\ \hat{\mathbf{c}}^\dagger \end{pmatrix} \;, \quad (7)$$

where the operator $\hat{c} = (\mathbf{c}_\uparrow, \mathbf{c}_\downarrow)$ and $\mathbf{c}_{\uparrow/\downarrow}$ is itself two component vector due to the two orbitals available in each lattice site. Ξ and Δ are , respectively, the kinetic energy and the pairing potential, both being 4×4 matrices, defined as:

$$\Xi = \begin{pmatrix} \mathbf{h}(\mathbf{k}).\tau + h_0(\mathbf{k}).\tau_0 & 0 \\ 0 & \mathbf{h}^*(-\mathbf{k}).\tau^* + h_0^*(-\mathbf{k}).\tau_0 \end{pmatrix} \quad (8)$$

$$\begin{cases} h_x = sin(k_y) \\ h_y = -sin(k_x) \\ h_z = 2t_1(cos(k_x) + cos(k_y)) + 4t_2 cos(k_x)cos(k_y) \\ h_0 = -\mu - t_1(cos(k_x) + cos(k_y)) \end{cases} \quad (9)$$

and

$$\hat{\Delta}(\mathbf{k}) = d_z(\mathbf{k})\sigma_x \otimes \tau_0 \text{ , with: } d_z(\mathbf{k}) = \Delta(sin(k_x) - isin(k_y)) \quad (10)$$

which is equivalent to

$$\hat{\Delta}(\mathbf{k}) = d_z(\mathbf{k}) \begin{pmatrix} 0 & \tau_0 \\ \tau_0 & 0 \end{pmatrix} \;, \quad (11)$$

and represents a p-wave superconducting paring. It can be proved that the topological properties of the superconductor do not stem from the topological properties of the kinetic energy and that non-trivial topology requires p-wave pairing.
The above choice for the pairing function breaks time-reversal symmetry. The system is therefore in the symmetry class D and has, for two spatial dimensions, a Z topological index, the Chern number [6].

The model describes a system in which the electrons with spin-up are paired with spin-down electrons, both having kinetic energies related by a time-reversal operation: $\Xi_\downarrow = \Xi_\uparrow^*(-\mathbf{k})$.
The matrix in eq(7) is the $\mathcal{H}_{BdG}$ Hamiltonian which has to satisfy the Bogolubov equations:

$$\begin{bmatrix} \Xi(\mathbf{k}) & \hat{\Delta}(\mathbf{k}) \\ \hat{\Delta}^\dagger(\mathbf{k}) & -\Xi^*(-\mathbf{k}) \end{bmatrix} \begin{pmatrix} u_\uparrow \\ u_\downarrow \\ v_\uparrow \\ v_\downarrow \end{pmatrix} = E \begin{pmatrix} u_\uparrow \\ u_\downarrow \\ v_\uparrow \\ v_\downarrow \end{pmatrix} \;, \quad (12)$$

in which u and v are both two component vectors accounting for the two orbitals available in each site. Writting explicity the equations resulting from eq(12) , allows to see that the $\mathcal{H}_{BdG}$ matrix only couples $u_\uparrow$ with $v_\downarrow$ and $u_\downarrow$ with $v_\uparrow$, showing that $\mathcal{H}_{BdG}$ can be decoupled into two separate systems: a 4×4 matrix for the $(u_\uparrow \;\; v_\downarrow)$ subspace and another 4×4 matrix which acts on the subspace $(u_\downarrow \;\; v_\uparrow)$.
In what follows, we shall only consider the subsystem $(u_\uparrow \;\; v_\downarrow)$:

$$\begin{bmatrix} \mathbf{h}(\mathbf{k}).\tau + h_0(\mathbf{k}).\tau_0 & d_z(\mathbf{k}).\tau_0 \\ d_z^*(\mathbf{k}).\tau_0 & -\mathbf{h}(\mathbf{k}).\tau - h_0(\mathbf{k}).\tau_0 \end{bmatrix} \begin{pmatrix} u_\uparrow \\ v_\downarrow \end{pmatrix} . \quad (13)$$

This Hamiltonian, eq(13), is in symmetry class A (unitary symmetry class) and has a Z topological index in two dimensions. It describes a spinful chiral p+ip superconductor [6].

$(u_\uparrow \quad v_\downarrow)$ are the eigenvectors of the system and can be written in the form:

$$\begin{bmatrix} u_\uparrow \\ v_\downarrow \end{bmatrix} = \begin{bmatrix} u_{\mathbf{k}} \begin{pmatrix} \alpha \\ \beta \end{pmatrix} \\ v_{\mathbf{k}} \begin{pmatrix} \alpha \\ \beta \end{pmatrix} \end{bmatrix} \tag{14}$$

where α and β are the orbital (pseudo-spin) eigenstates of the Bloch Hamiltonian h.

Distinct choices of the Hamiltonian parameters can lead to distinct topological phases and thus different Chern numbers. Fixing $\mu = 0.7$ and $\Delta = 0.1$, a topological state will have to be probed by varying the hopping parameters t_1 and t_2. Choosing $t_1 = 0.07$ with t_2 either $+0.08$ or -0.08 and calculating the Chern number for each choice, one obtains:

$$\begin{cases} t_2 = -0.08 \Rightarrow C = 1 \Rightarrow & \text{Topological phase} \\ t_2 = 0.08 \Rightarrow C = 0 \Rightarrow & \text{Trivial phase} \end{cases} . \tag{15}$$

To compute the Chern number, the method developed by Fukui, Hatsugai and Suzuki for multiband superconductors [20, 21] was implemented.
In eq(15) the Fermi surfaces are not the same in each phase. When topology is present, the Fermi surface contains 3 electron pockets centered at momentum coordinates ($k_x = 0$, $k_y = 0$) , ($k_x = 0$, $k_y = \pi$) , ($k_x = \pi$, $k_y = 0$). In the trivial phase, the Fermi surface will contain another pocket located at ($k_x = \pi$, $k_y = \pi$), fig(1).

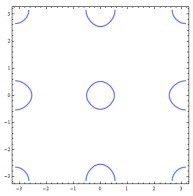

(a) Fermi surface for $t_2 = 0.08$ with 4 electron pockets.

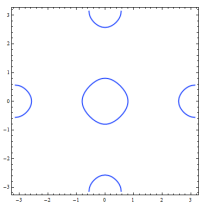

(b) Fermi surface for $t_2 = -0.08$ with 3 electron pockets.

Figure 1: Fermi surfaces for the two choices of the parameter t_2

The number of edge states is related to the nontrivial topology of the system. This is the bulk-boundary correspondence (eq.(1)). Thus, if $C = 1$ there can only precisely exist a single Majorana fermion (fig.(2)) and one must expect to infer its existence by solely indentifying one ABS in the differential conductance.

3. Quantum waveguide theory of Andreev spectroscopy

To study the scattering processes occurring at an interface between a normal metal and a multiband superconductor a new theory must be introduced, such that the quantum interference between transmitted waves into the superconductor is taken into account. The incoming electron from the single band metal has to split into two conduction channels in the two-band superconductor. This situation is analogous to a waveguide [18], leading the authors M.A.N. Araújo and P.D. Sacramento to adapt the quantum waveguide problem to treat the matching conditions at the interface between a normal metal and a multiband superconductor [16].
Assuming the edge of the superconductor to be along the y direction, an incident electron wavevector with an arbitrary angle with respect to the interface normal vector, will have its vector components parallel to the interface conserved in the scattering processes, allowing to impose the boundary conditions in the same limit as in a one-dimensional problem. This means that in the xy plane, the boundary conditions at the interface will be probed in the limit $x \to 0$.

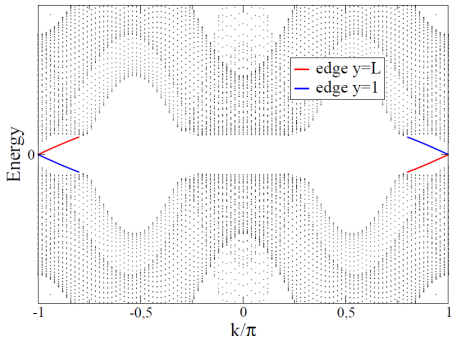

Figure 2: Energy spectrum of the Hamiltonian model eq(7) for an infinite ribbon in the yy (or xx) direction. The Majorana Fermion can be seen for the longitudinal momentum π. This figure was obtained by M.A.N. Araújo.

Recalling that we are only considering the subsystem $(u_\uparrow \quad v_\downarrow)$, we follow eqs(13) and (14) for the wavefunctions in the superconductor and write:

$$\begin{pmatrix} \mathbf{h}(\mathbf{k}).\tau + h_0(\mathbf{k}).\tau_0 & d_z(\mathbf{k}).\tau_0 \\ d_z(\mathbf{k})^*\tau_0 & -\mathbf{h}(\mathbf{k}).\tau - h_0(\mathbf{k}).\tau_0 \end{pmatrix} \begin{pmatrix} u\alpha \\ u\beta \\ v\alpha \\ v\beta \end{pmatrix} = E \begin{pmatrix} u\alpha \\ u\beta \\ v\alpha \\ v\beta \end{pmatrix} \tag{16}$$

As the y component of the wavevector is a conserved quantity, one can construct the transmited wavefunction in the superconductor's region as $e^{ip_y y}\Psi_S$, where

$$\Psi_S(x \geq 0) = C\psi_{\mathbf{k}^+}e^{ik^+x} + D\psi_{\mathbf{k}^-}e^{-ik^-x} + E\psi_{\mathbf{q}^+}e^{iq^+x} + F\psi_{\mathbf{q}^-}e^{-iq^-x} \tag{17}$$

Each $\psi_{\mathbf{k}}$ denotes a four-dimensional column eigenvector of the BdG matrix from eq(16). The transmited excitations are superpositions of the wave-vectors $\mathbf{k}_{\pm}$ and $\mathbf{q}_{\pm}$ from the two Fermi-surface pockets. Their x-component is chosen such that the group velocity is positive for an energy E above the energy gap. For the normal-metal, which is a single-band metal, the wavefunction is given by $e^{ip_y y}\Psi_N$ with:

$$\Psi_N(x \leq 0) = e^{ip^+x}\begin{pmatrix}1\\0\end{pmatrix} + be^{-ip^+x}\begin{pmatrix}1\\0\end{pmatrix} + ae^{ip^-x}\begin{pmatrix}0\\1\end{pmatrix} \tag{18}$$

In the approximation where $k^{\pm}$ and $q^{\pm}$ both take the value of their respective Fermi momentum, their determination can be achieved by finding the zeros of the electron-like energy band, which are closest to the center of correspondent Fermi-pocket.
With both wavefunctions in each region specified, one can now proceed by applying the waveguide boundary conditions. The first boudary condition imposes the wavefunction to be single valued at the node (interface) and follows immediatly if one evaluates the wavefunctions, in each region, in the limit $x \to 0$:

$$\begin{cases} Cu_{\mathbf{k}^+}\alpha_{\mathbf{k}^+} + Du_{\mathbf{k}^-}\alpha_{\mathbf{k}^-} + Eu_{\mathbf{q}^+}\alpha_{\mathbf{k}^+} + Fu_{\mathbf{q}^-}\alpha_{\mathbf{q}^-} \\ = 1 + b \\ Cu_{\mathbf{k}^+}\beta_{\mathbf{k}^+} + Du_{\mathbf{k}^-}\beta_{\mathbf{k}^-} + Eu_{\mathbf{q}^+}\beta_{\mathbf{k}^+} + Fu_{\mathbf{q}^-}\beta_{\mathbf{q}^-} \\ = 1 + b \\ Cv_{\mathbf{k}^+}\alpha_{\mathbf{k}^+} + Dv_{\mathbf{k}^-}\alpha_{\mathbf{k}^-} + Ev_{\mathbf{q}^+}\alpha_{\mathbf{k}^+} + Fv_{\mathbf{q}^-}\alpha_{\mathbf{q}^-} \\ = a \\ Cv_{\mathbf{k}^+}\beta_{\mathbf{k}^+} + Dv_{\mathbf{k}^-}\beta_{\mathbf{k}^-} + Ev_{\mathbf{q}^+}\beta_{\mathbf{k}^-} + Fv_{\mathbf{q}^-}\beta_{\mathbf{q}^-} \\ = a \end{cases} \tag{19}$$

The second boundary condition imposes the conservation of current at the interface. It shall be used the definition for the probability current given in reference [16]:

$$\mathbf{j}(\mathbf{r}) = Re\{\psi^{\dagger}(\mathbf{r})\frac{\partial \hat{H}}{\partial \hat{\mathbf{k}}}\psi(\mathbf{r})\}\text{ , with: }\hat{\mathbf{k}} = -i\nabla\ . \tag{20}$$

Then, the condition for current conservation may be imposed as:

$$\lim_{n\to 0^-}\Big(\frac{\partial E_{nomal\ metal}}{\partial \hat{p}}\psi_{inc}\Big) \tag{21}$$

$$= (1\ \ 1).\lim_{n\to 0^+}\Big(\frac{\partial \mathcal{H}_{BdG\,(u_\uparrow, v_\downarrow)}}{\partial \hat{\mathbf{k}}}\psi_{trans}\Big)\ , \tag{22}$$

where $\mathcal{H}_{BdG\,(u_\uparrow, v_\downarrow)}$ represents the matrix from eq(16). Thus, the current conservation at the node can be expressed as:

$$\begin{cases} 1 - b = C\Theta(\mathbf{k}^+) + D\Theta(\mathbf{k}^-) + E\Theta(\mathbf{q}^+) + F\Theta(\mathbf{q}^-) \\ a = C\Phi(\mathbf{k}^+) + D\Phi(\mathbf{k}^-) + E\Phi(\mathbf{q}^+) + F\Phi(\mathbf{q}^-)\ , \end{cases} \tag{23}$$

where $\Theta(\mathbf{k})$ and $\Phi(\mathbf{k})$ are the auxiliar functions defined as follow:

$$\Theta = \frac{m}{p^+}(1,1).\Big(u_{\mathbf{k}}\frac{\partial\{\mathbf{h}(\mathbf{k}).\tau + h_0(\mathbf{k}).\tau_0\}}{\partial k_x} \tag{24}$$

$$+v_{\mathbf{k}}\frac{\partial d_z(\mathbf{k})}{\partial k_x}\Big)\begin{bmatrix}\alpha_{\mathbf{k}}\\ \beta_{\mathbf{k}}\end{bmatrix}\ . \tag{25}$$

$$\Phi = \frac{m}{p^-}(1,1).\Big(v_{\mathbf{k}}\frac{\partial\{\mathbf{h}(\mathbf{k}).\tau + h_0(\mathbf{k}).\tau_0\}}{\partial k_x} - u_{\mathbf{k}}\frac{\partial d_z^*(\mathbf{k})}{\partial k_x}\Big)\begin{bmatrix}\alpha_{\mathbf{k}}\\ \beta_{\mathbf{k}}\end{bmatrix}\ . \tag{26}$$

From eq(19) it is possible to invert the system and attain the amplitudes C, D, E and F in terms of a and b:

$$\begin{cases} C = \frac{(1+b)\Gamma_1 + a\Gamma_2}{\Lambda} \\ D = \frac{(1+b)\Gamma_3 + a\Gamma_4}{\Lambda} \\ E = \frac{(1+b)\Gamma_5 + a\Gamma_6}{\Lambda} \\ F = \frac{(1+b)\Gamma_7 + a\Gamma_8}{\Lambda} \end{cases} \tag{27}$$

$$\text{with: }\Lambda = \begin{vmatrix} u_{\mathbf{k}^+}\alpha_{\mathbf{k}^+} & u_{\mathbf{k}^-}\alpha_{\mathbf{k}^-} & u_{\mathbf{q}^+}\alpha_{\mathbf{k}^+} & u_{\mathbf{q}^-}\alpha_{\mathbf{q}^-} \\ u_{\mathbf{k}^+}\beta_{\mathbf{k}^+} & u_{\mathbf{k}^-}\beta_{\mathbf{k}^-} & u_{\mathbf{q}^+}\beta_{\mathbf{k}^+} & u_{\mathbf{q}^-}\beta_{\mathbf{q}^-} \\ v_{\mathbf{k}^+}\alpha_{\mathbf{k}^+} & v_{\mathbf{k}^-}\alpha_{\mathbf{k}^-} & v_{\mathbf{q}^+}\alpha_{\mathbf{k}^+} & v_{\mathbf{q}^-}\alpha_{\mathbf{q}^-} \\ v_{\mathbf{k}^+}\beta_{\mathbf{k}^+} & v_{\mathbf{k}^-}\beta_{\mathbf{k}^-} & v_{\mathbf{q}^+}\beta_{\mathbf{k}^-} & v_{\mathbf{q}^-}\beta_{\mathbf{q}^-} \end{vmatrix} \tag{28}$$

The coefficients Γ_i are given by linear combinations of the cofactor elements C_{lj} that form the inverse matrix of system (19). For example, $\Gamma_1 = C_{11} + C_{12}$.
It is now explicit that the reflection and the Andreev amplitudes will become dependent on the determinant of the matrix Λ. Futhermore,when $\Lambda \to 0$,these amplitudes will become independent of the barrier strength, with the transmission occuring via the localized ABS.
It is still necessary to introduce the effect of the repulsive potential at the interface. The problem can be more easily addressed if the repulsive potential is slightly shifted from the node point, thus allowing it to be treated at the normal single-band region. This procedure leads to the replacements:

$$1 - b \to 1 - b - 2iZ(1+b)\frac{p_F}{p^+} \tag{29}$$

$$a \to a(1 - 2iZ\frac{p_F}{p^-}) \tag{30}$$

With these replacements plus eq(27), it is possible to rewrite the equations coming from the boundary condition for current conservation as:

$$\begin{cases} (1-b) - 2iZ\frac{p_F}{p^+}(1+b) = \frac{1}{\Lambda}(\zeta_{11}(1+b) + a\zeta_{12}) \\ a(1 - 2iZ\frac{p_F}{p^-}) = \frac{1}{\Lambda}(\zeta_{21}(1+b) + a\zeta_{22}) \ , \end{cases} \tag{31}$$

where ζ_{ij}, $(i,j) = \{1,2\}$ are the quantities defined as:

$$\begin{cases} \zeta_{11} = \Gamma_1\Theta(\mathbf{k}^+) + \Gamma_3\Theta(\mathbf{k}^-) + \Gamma_5\Theta(\mathbf{q}^+) + \Gamma_7\Theta(\mathbf{q}^-) \\ \zeta_{12} = \Gamma_2\Theta(\mathbf{k}^+) + \Gamma_4\Theta(\mathbf{k}^-) + \Gamma_6\Theta(\mathbf{q}^+) + \Gamma_8\Theta(\mathbf{q}^-) \\ \zeta_{21} = \Gamma_1\Phi(\mathbf{k}^+) + \Gamma_3\Phi(\mathbf{k}^-) + \Gamma_5\Phi(\mathbf{q}^+) + \Gamma_7\Phi(\mathbf{q}^-) \\ \zeta_{22} = \Gamma_2\Phi(\mathbf{k}^+) + \Gamma_4\Phi(\mathbf{k}^-) + \Gamma_6\Phi(\mathbf{q}^+) + \Gamma_8\Phi(\mathbf{q}^-) \ . \end{cases} \tag{32}$$

Solving the system of eqs(31), one obtains the final form for the amplitudes of normal and Andreev reflection:

$$a = \frac{2\zeta_{21}\Lambda}{(1 + 2iZ + \frac{\zeta_{11}}{\Lambda})(1 - 2iZ - \frac{\zeta_{22}}{\Lambda}) + \frac{\zeta_{12}\zeta_{21}}{\Lambda^2}} \tag{33}$$

$$b = \frac{(1 - 2iZ - \frac{\zeta_{11}}{\Lambda})(1 - 2iZ - \frac{\zeta_{22}}{\Lambda}) - \frac{\zeta_{12}\zeta_{21}}{\Lambda^2}}{(1 + 2iZ + \frac{\zeta_{11}}{\Lambda})(1 - 2iZ - \frac{\zeta_{22}}{\Lambda}) + \frac{\zeta_{12}\zeta_{21}}{\Lambda^2}} \tag{34}$$

It is then possible to calculate the differential conductance of the N-S junction, $g_s = 1 + |a|^2 - |b|^2$.

4. Differential conductance of the N-S boundary

All the above construction can be applied to determine the behavior of the differential conductance g_s as a function of the bias voltage. Particularly, g_s will be computed in two distinct choices for the Hamiltonian parameter t_2 ($t_2 = +0.08$ and $t_2 = -0.08$) which, as mentioned before, lead the system into two distinct phases: a trivial and a topological phase, respectively. For the transverse momentum fixed at normal incidence, $p_y = 0$, and considering the non-topological case, waveguide theory provides the results in fig(3)-(5) , which account for different magnitudes of the strength barrier, Z.

As one may see, the electron transport at zero energy-bias $E \to 0$ is supressed, even though excitations k^+ and q^+ are submitted to a sign-reversed pairing potential version of their correspondent counterpart k^- and q^- , which might lead to expect a similiar situation as in d-wave superconductivity. Also, the observed vanishment of g_s for $E \to 0$ becomes more pronounced with the increase of the disorder parameter Z.

If one applies the generalized form of BTK theory for an anisotropic pair potential, one will attain an ABS at zero energy in each Fermi-pocket , identifiable by the condition: $\Lambda \to 0$. This condition was never satisfied for the differential conductances attained with waveguide theory for $t_2 = +0.08$.

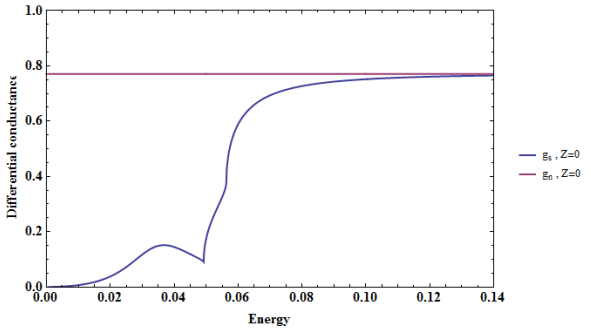

Figure 3: Conductance g_s (blue) and g_n (red) as function of the incident electron energy for $t_2 = +0.08$ in a microconstriction, Z=0, for a fixed transverse momentum $p_y = 0$. Calculation performed with waveguide theory.

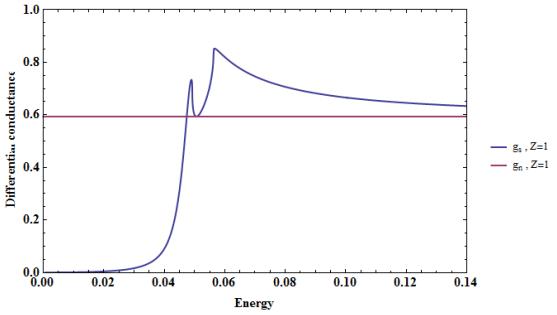

Figure 4: Conductance g_s (blue) and g_n (red) as function of the incident electron energy for $t_2 = +0.08$ and Z=1, for a fixed transverse momentum $p_y = 0$. Calculation performed with waveguide theory.

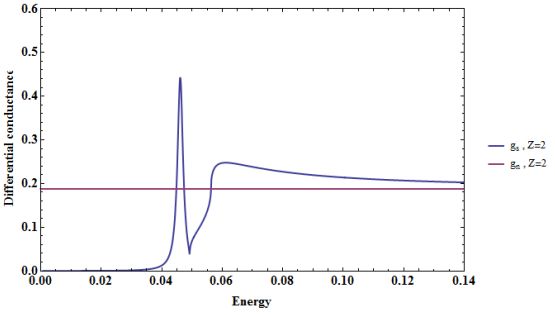

Figure 5: Conductance g_s (blue) and g_n (red) as function of the incident electron energy for $t_2 = +0.08$ and Z=2, for a fixed transverse momentum $p_y = 0$. Calculation performed with waveguide theory.

With the same choice of the parameter t_2 , but altering the transversed momentum to $p_y = \pi$, waveguide theory predicts the behaviour of the dif-

ferential conductances in fig(6)-(8) . Similarly to $p_y = 0$ there are no bound states and the conductivity at zero bias energy is supressed.

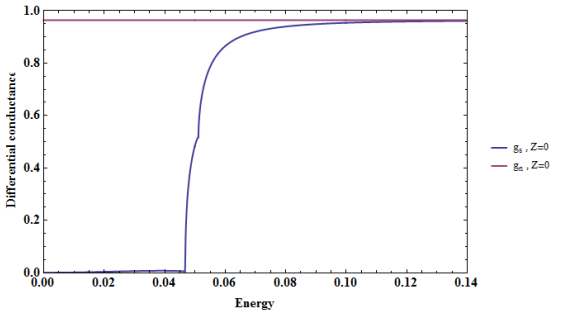

Figure 6: Conductance g_s (blue) and g_n (red) as function of the incident electron energy for $t_2 = +0.08$ and Z=0, for a fixed transverse momentum $p_y = \pi$. Calculation performed with waveguide theory.

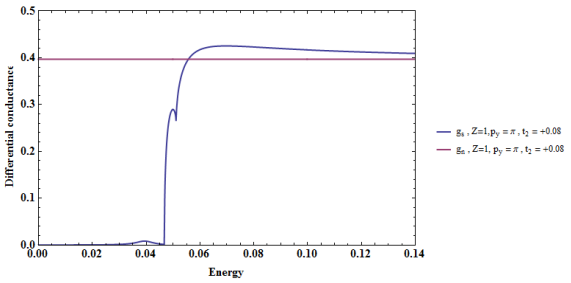

Figure 7: Conductance g_s (blue) and g_n (red) as function of the incident electron energy for $_t2 = +0.08$ and Z=1, for a fixed transverse momentum $p_y = \pi$. Calculation performed with waveguide theory.

Furthermore, the assymptotic behaviour of the differential conductance g_s as the bias energy increases is similar in all the present figures: it becomes increasingly closer to the normal conductance g_n , illustrating that the special features of the N-S juction are circumscribed to a range of energies near the gap energy.

For the topological phase, considering a normal incidence, $p_y = 0$, and applying quantum waveguide theory provides a similar qualitative picture as for $t_2 = +0.08$, with also zero conductance at $E \to 0$.

Likewise, applying the extended version of the BTK theory in this case results in the opposite prediction with an enhanced flow of current occuring at zero bias and detecting the presence of an ABS which would be a Majorana fermion, due to topology. The model also grants the same conclusion if rather than a normal incidence, the transverse momentum is fixed at $p_y = \pi$. Thus BTK theory predicts the existence of a Majorana Fermion in each Fermi pocket, a contradiction with the topological properties of the system which only allow one Majorana Fermion.

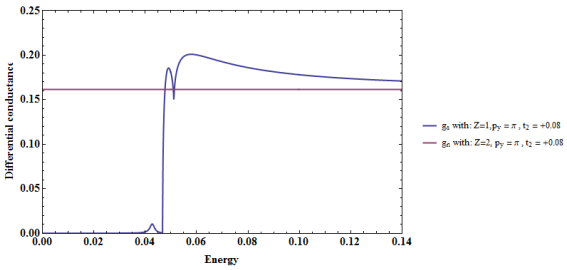

Figure 8: Conductance g_s (blue) and g_n (red) as function of the incident electron energy for $_t2 = +0.08$ and Z=2, for a fixed transverse momentum $p_y = \pi$. Calculation performed with waveguide theory.

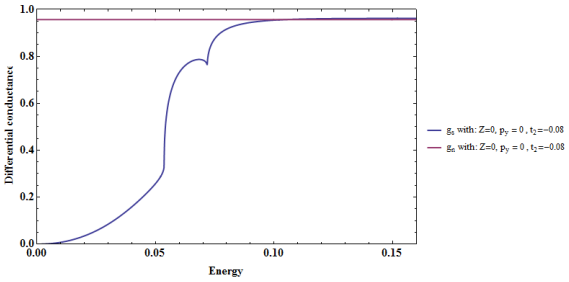

Figure 9: Conductance g_s (blue) and g_n (red) as function of the incident electron energy for $t_2 = -0.08$ and Z=0 and a fixed transverse momentum $p_y = 0$. Calculation performed with waveguide theory.

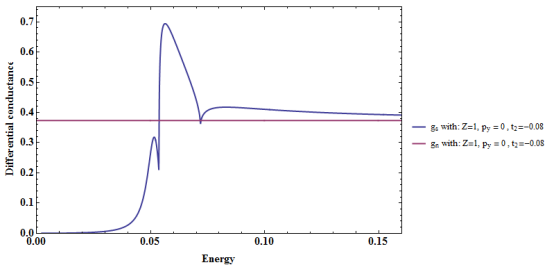

Figure 10: Conductance g_s (blue) and g_n (red) as function of the incident electron energy for $_t2 = -0.08$ and Z=1 and a fixed transverse momentum $p_y = 0$. Calculation performed with waveguide theory.

The differential conductance attained by waveguide theory with fixed transverse momentum $p_y = \pi$ and $t_2 = -0.08$, however, breaks the pattern of sup-

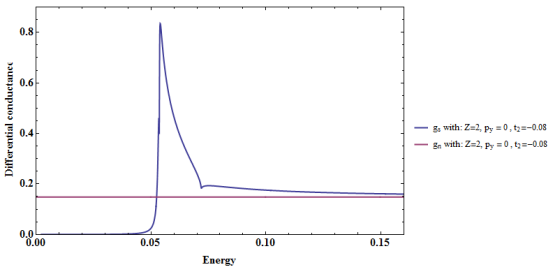

Figure 11: Conductance g_s (blue) and g_n (red) as function of the incident electron energy for $t_2 = -0.08$ and Z=2 and a fixed transverse momentum $p_y = 0$. Calculation performed with waveguide theory.

pressed zero bias conductivity and meets for the first time the criterium for ABS.

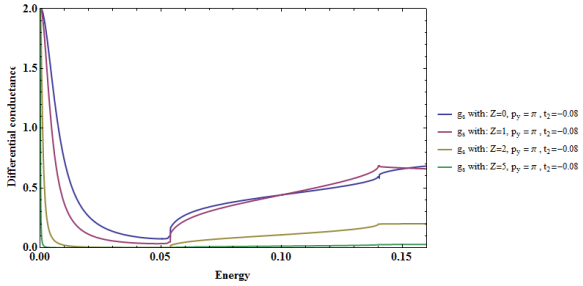

Figure 12: Conductance g_s as function of the incident electron energy for $t_2 = -0.08$ with various strength barriers: Z=0 (blue), Z=1 (red), Z=2 (yellow) , Z=5 (green). The transverse momentum is fixed at the value $p_y = \pi$. Calculation performed using waveguide theory.

One can observe that the enhanced peak located at zero energy is conserved even when the barrier parameter increases to $Z = 5$, therefore being independent of the local interface disorder, which is exactly what one would expect for an ABS. Because the parameter choice imposes a topological phase, the localized ABS can be identified as a Majorana fermion.

With all these considerations, it is then possible to conclude that in order to attain consistency between the topological properties of the system and the number of ABS in each Fermi-pocket, it is necessary that an interference effect occurs between the two traversed Fermi pockets, fixed by the momentum p_y. These interference effects are correctly accounted for by the waveguide theory, emphasizing the importance of taking into account from the start the various conduction channels at a multiband superconductor, rather than treating them independently and constructing the final differential conductance as a sum of all separate contributions. Furthermore, when applied to a single pocket, waveguide theory proved to attain the correct behaviour expected in the presence of ABS.

5. Conclusions

For the choice of the Hamiltonian's parameter $t_2 = -0.08$, the Fermi surface is composed by an odd number of electron pockets and quantum waveguide theory allows a differential conductivity with a zero-energy ABS located at the single pocket, which can be identified as a Majorana fermion because with such value of t_2 the system is in a topological phase with $C = 1$. This ABS is also present when the differential conductance of the single-pocket is attained in the BTK framework, although the theory also predicts an ABS in each of the other electron-pockets even when the system is non-topological. This suggests that for the number of ABS to be reconciled with the topological properties of the system, the two ABS states predicted by BTK theory for the pockets $(0, 0)$ and $(\pi, 0)$ should interfere destructively when the incident electron has transverse momentum $p_y = 0$. For quantum waveguide theory this is exactly what is observed. Thus, quantum waveguide correctly integrates the number of calculated ABS with the topological features of the model, revealing the presence of important quantum interference effects suppressing conductivity at zero energy bias, when two real electron pockets are transversed, a phenomena which will not be observed if the bands are treated as separate conduction channels and added together to form the differential conductivity at the interface.

As future work it would be interesting to study: the effect of spin-orbit interaction, by introducing a Rabash term in the Hamiltonian. The Rabash spin-orbit term can lead to the recent discovered phenomena of selective equal spin Andreev reflection [22], which consists of incident electrons, with certain spin orientations, being reflected as holes with the same spin, at the interface between a normal-metal and a topological superconductor; or calculate the differential conductance g_s for the crossed Andreev reflection mechanism.

References

[1] Jan Carl Budich and Björn Trauzettel, From adiabatic theorem of quantum mechanics to topological states of matter, Physica Status Solidi (RRL) - Rapid Research Letters,7,109 (2013).

[2] M. Z. Hasan and C. L. Kane, Colloquium: Topological insulators, Reviews of Modern Physics, 82, 3045, (2010).

[3] B. Andrei Bernevig and Taylor L.Hughes, Topological Insulators and Topological Super-

conductors, Princeton University Press (2013).

[4] Xue-Feng Wang, Yibin Hu, and Hong Guo, Robustness of the helical edge states in topological insulators, Phys. Rev. B, 85, 241402(R) (2012).

[5] M.V.Berry and F.R.S., Quantal phase factors accompanying adiabatic changes, Proc.R.Soc.London A, 392, 45 (1983).

[6] Andreas P. Schnyder, Shinsei Ryu, Akira Furusaki and Andreas W.W. Ludwig, Classification of topological insulators and superconductors in three spatial dimensions, Physical Review B, 78, 195125 (2008).

[7] Manfred Sigrist and Kazuo Ueda, Phenomenological theory of unconventional superconductivity, Reviews of Modern Physics, 63, 239 (1991).

[8] P.G. De Gennes, Superconductivity of Metals and Alloys, Oxford Science Publications (2012).

[9] Jason Alicea, New directions in the pursuit of Majorana fermions in solid state systems, Rep. Prog. Phys., 75, 076501 (2012).

[10] Martin Leijnse and Karsten Flensberg, Introduction to topological superconductivity and Majorana fermions, Semiconductor Science and Technology, 27 , 124003 (2012).

[11] Shinsei Ryu, Hunting Majorana Fermions in Topological Superconductors, Journal of the Physical Society of Japan, News Comments 11, 11 (2014).

[12] E.L.Wolf, Principles of Electron Tunneling Spectroscopy, Oxford Science Publications (2012).

[13] G. E. Blonder, M. Tinkham and T. M. Klapwijk, Transition from metallic to tunneling regimes in superconducting microconstrictions: Excess current, charge imbalance and supercurrent conversion, Physical Review B, 7, 4515 (1982).

[14] Satoshi Kashiwaya, Yukio Tanaka, Masao Koyanagi and Koji Kajimura, Theory for tunneling spectroscopy of anisotropic superconductors, Physical Review B, 53, 2667 (1996).

[15] Chia-Ren Hu, Midgap Surface States as a Novel Signature for $d_{x_a^2-x_b^2}$ -Wave Superconductivity, Physical Review Letters, 72, 1526 (1994).

[16] M. A. N. Araú jo and P. D. Sacramento, Quantum waveguide theory of Andreev spectroscopy in multiband superconductors: the case of Fe-pnictides, Physical Review B, 79, 174529 (2009).

[17] Jacob Linder and Asle Sudb, Theory of Andreev reflection in junctions with iron-based high-T_c superconductors, Physical Review B, 79, 020501(R) (2009).

[18] Jian-Bai Xia, Quantum waveguide theory for mesoscopic structures, Physical Review B, 45, 3593 (1992).

[19] M.A.N.Araújo and P. D. Sacramento, Electron transmission in normal metal/heavy-fermion superconductor junctions: A two-band model, Physical Review B, 77, 134519 (2008).

[20] Yasuhiro Hatsugai, Takahiro Fukui and Hideo Aoki, Topological analysis of the quantum Hall effect in graphene: Dirac-Fermi transition across van Hove singularities and edge versus bulk quantum numbers, Physical Review B, 74, 205414 (2006).

[21] Takahiro Fukui, Yasuhiro Hatsugai and Hiroshi Suzuki, Chern Numbers in Discretized Brillouin Zone: Efficient Method of Computing (Spin) Hall Conductances, J. Phys. Soc. Jpn., 74 , 1674 (2005).

[22] James J. He,T. K. Ng,Patrick A. Lee and K. T. Law, Selective Equal-Spin Andreev Reflections Induced by Majorana Fermions, Physical Review Letters, 112, 037001 (2014).